# Modelling Analysis of HTS CICCs

## Quench anslysis of the BEST CS HTS conductor

**Monika LEWANDOWSKA[1,2], Aleksandra DEMBKOWSKA[1,2]**

1. The Henryk Niewodniczański Institute of Nuclear Physics
Polish Academy of Sciences, Kraków, Poland

2. West Pomeranian University of Technology in Szczecin, 70-310 Szczecin, Poland

**EU-CN Collaboration Meeting, Rome, 28 October 2026**

# Outline

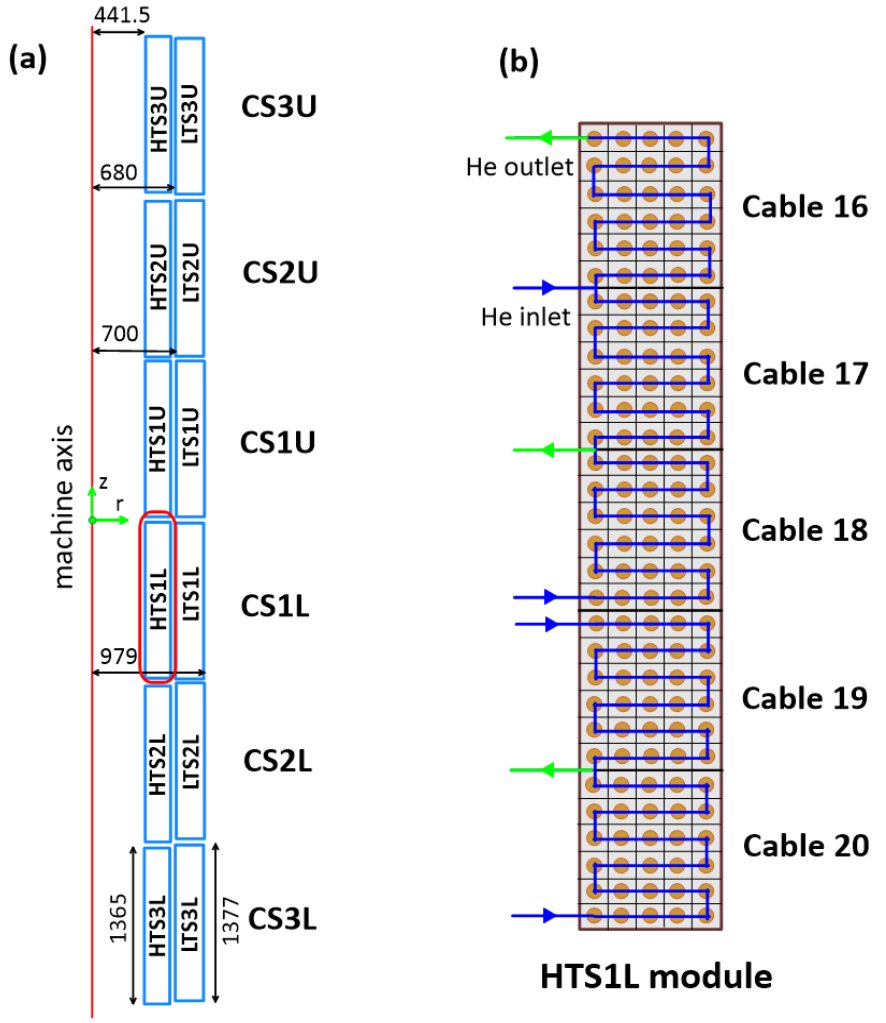
- Goal of the study
- Input data and model assumptions
  - Magnetic flux distribution within the CS coil
  - THEA model
  - AC losses evaluation
  - Quench simulations assumptions
- Results and discussion
- Summary and conclusion

# Goal of the study

- Estimation of the maximum hot spot temperature during quench of the HTS CORC CS conductor and verification if it fulfills the acceptance criterion:

$$\max T_{jacket} < 150\ K$$

# Input data – CS coils and HTS conductor geometry



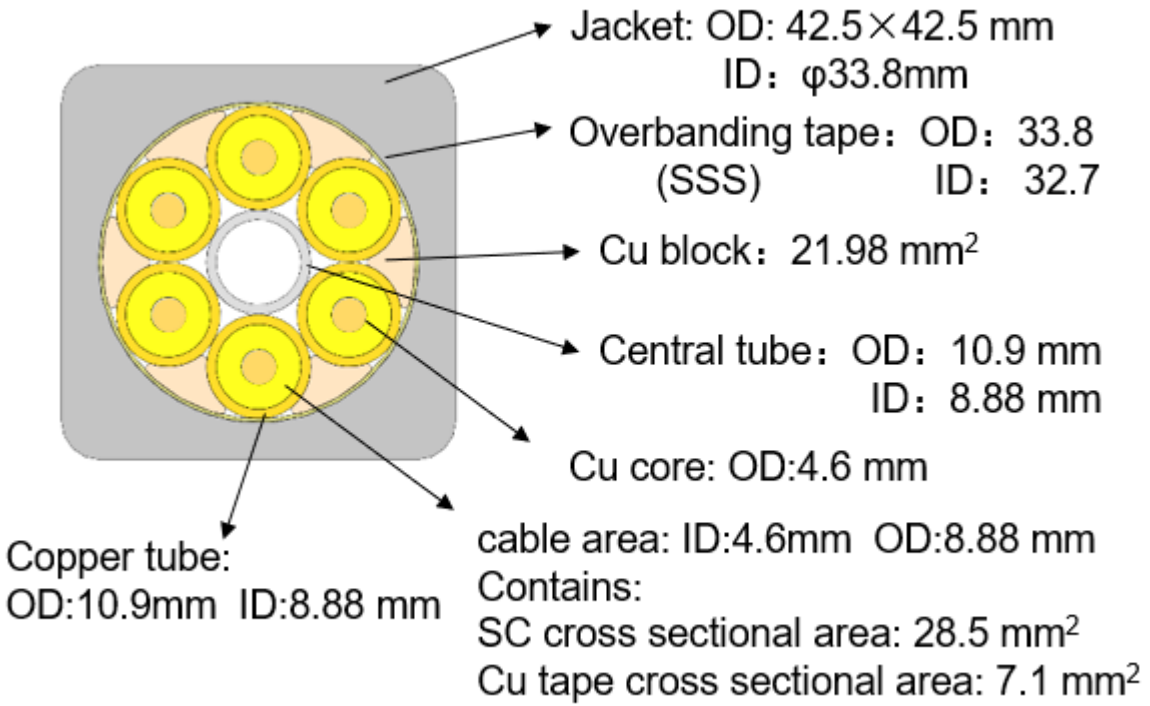
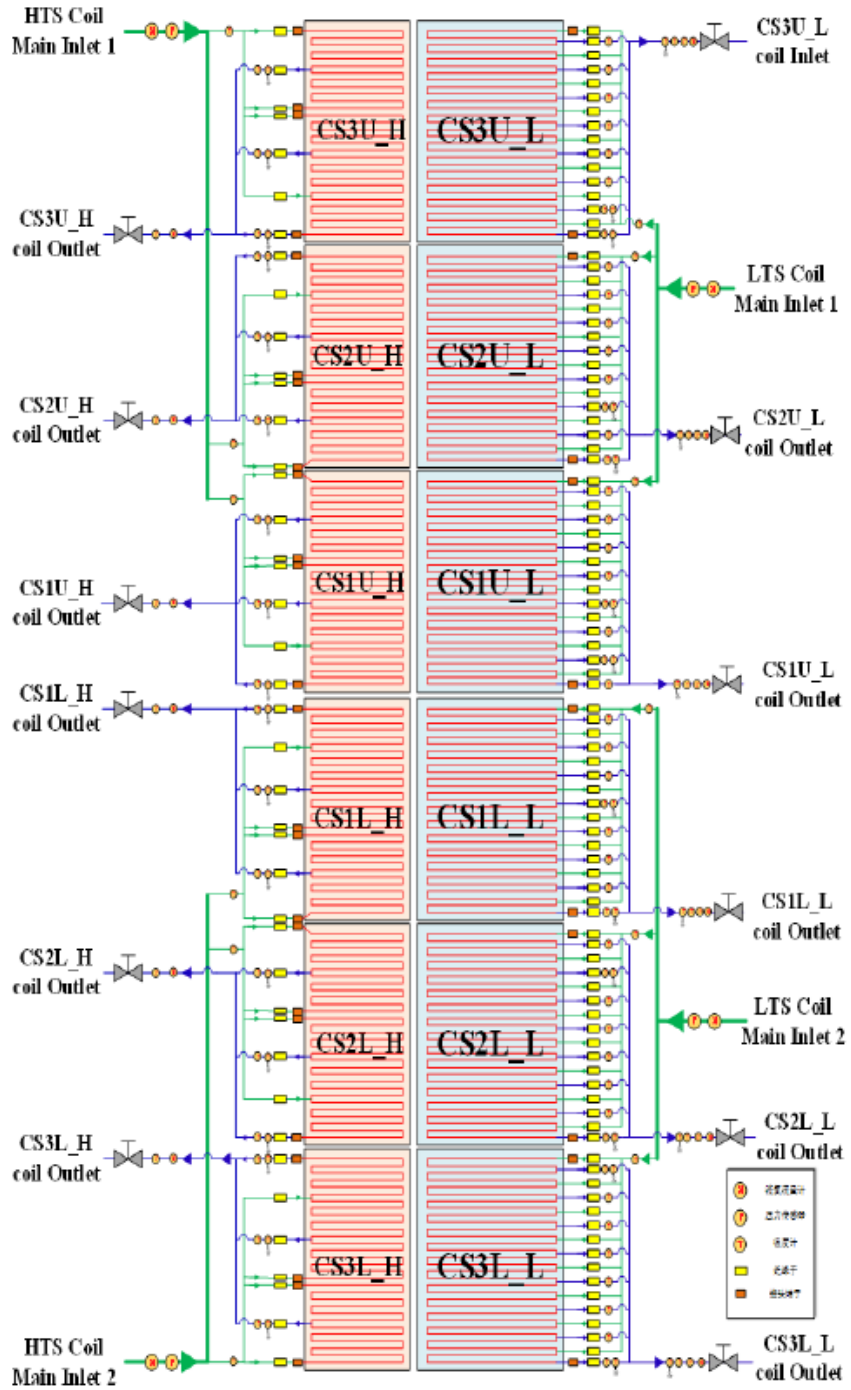
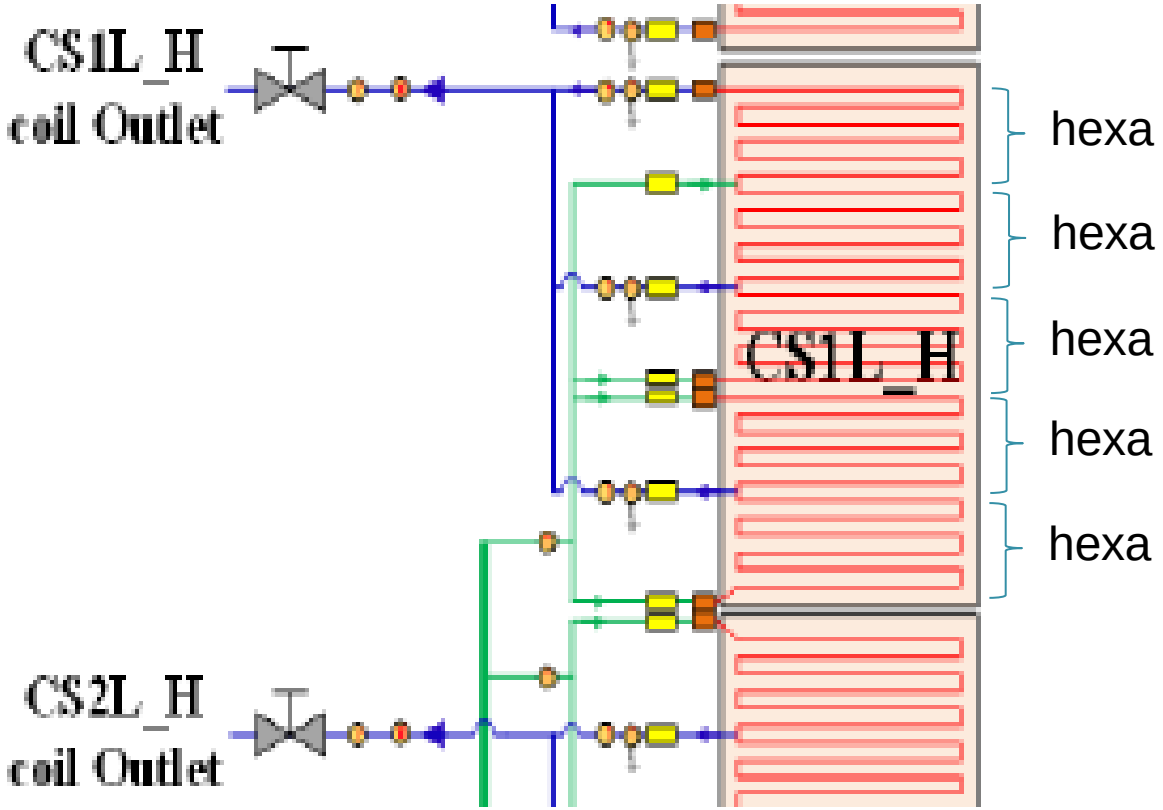




Figure 1. (a) Locations and size of the CS modules (dimensions in mm), (b) Schematic cross section of one of the HTS modules and scheme of its cooling circuit (conductors are numbered starting from the top of the CS).

- Max. operating current: 46.5 kA
- Number of HTS tapes: $n_t$ = 288
- HTS tapes width: 4 mm
- He cross section (central channel): 28.74 mm²
- He cross section (6 triangle channels): 28.74 mm²

# Input data – cooling conditions




He inlet pressure: 5 bar

He inlet temperature: 4.2 K

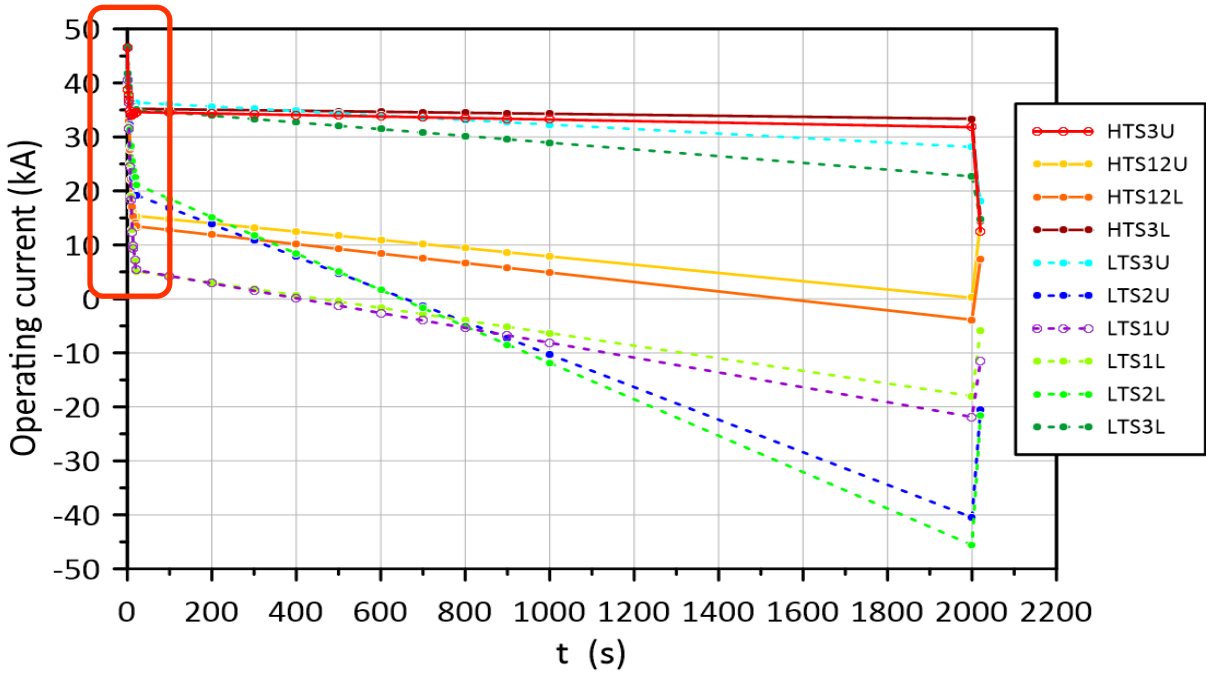
Nominal mass flow rate: 14 g/s (at no heat load)

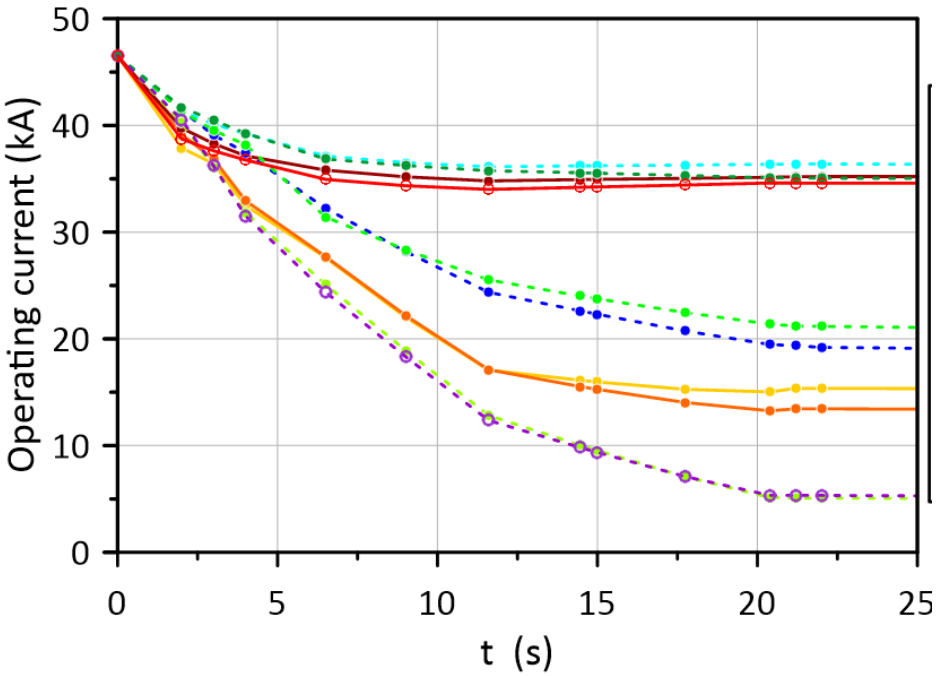
5 Hexa-pancakes in each HTS module

5 Turns in each pancake

Hydraulic length ~ 106 m

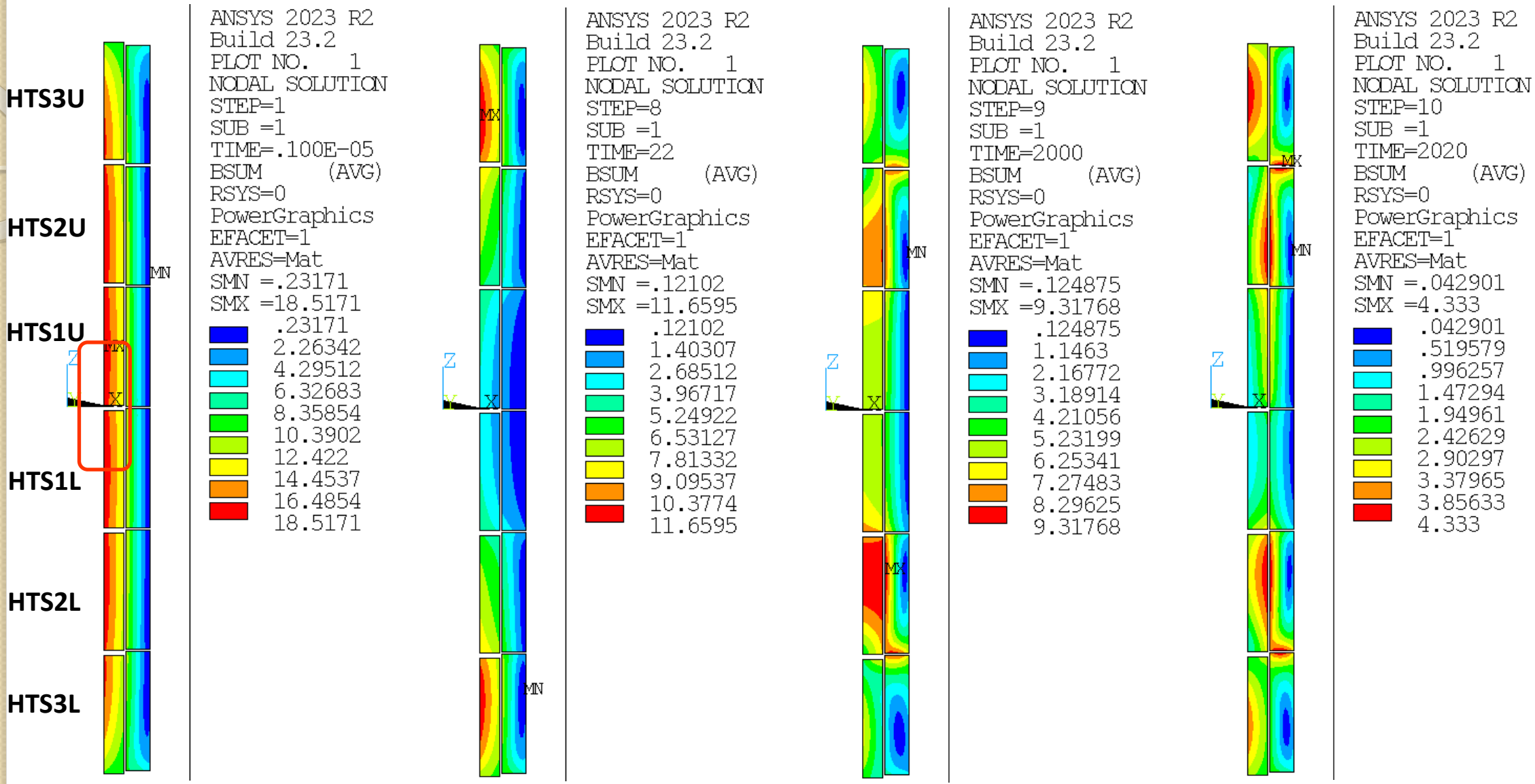
# Input data – normal current scenario




We developed an axisymmetric model of the CS in the ANSYS APDL environment to calculate the magnetic field distribution within the CS at 10 (out of 25) time points selected from the current scenario (namely: t = 0, 2, 3, 4, 6.5, 11.4, 20.4, 22, 2000, and 2020 s), between which the operating current in CS conductors varied almost linearly.

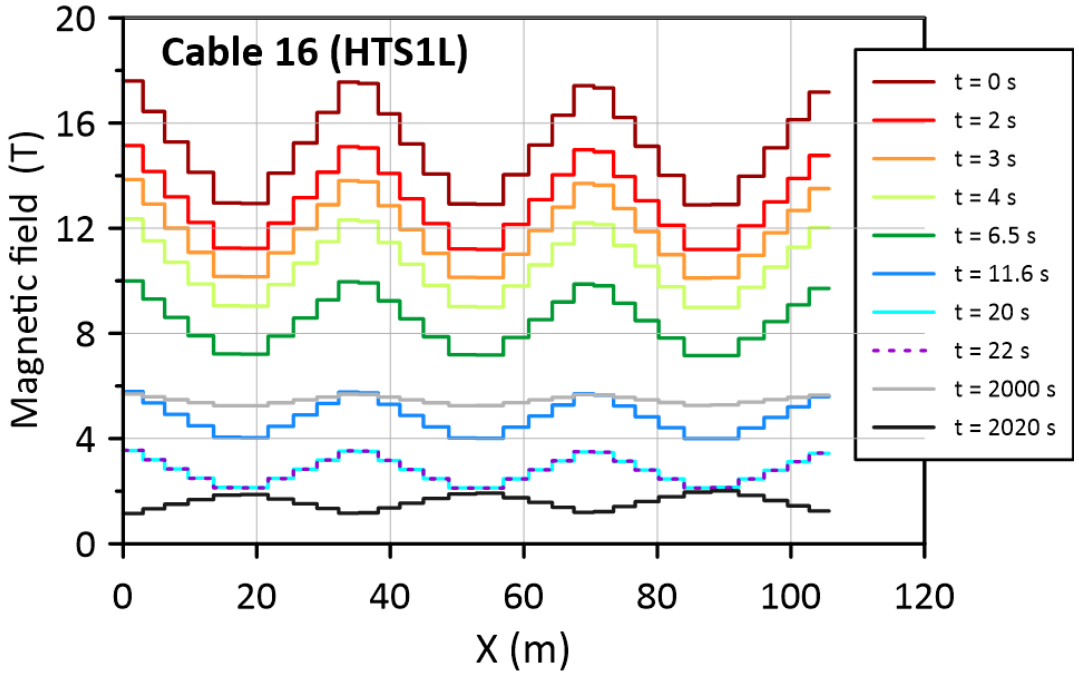
# Magnetic field evolution in the CS modules



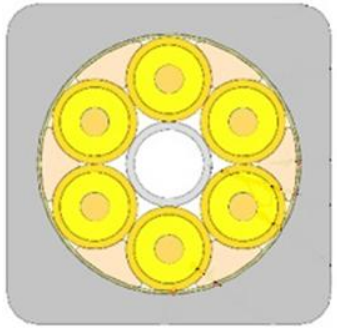

[1] M. Lewandowska, et al., *Thermal-hydraulic analysis of the HTS part of the hybrid Central Solenoid designed for the next generation experimental fusion device*. Fusion Engineering and Design. 232 (2026) 116028

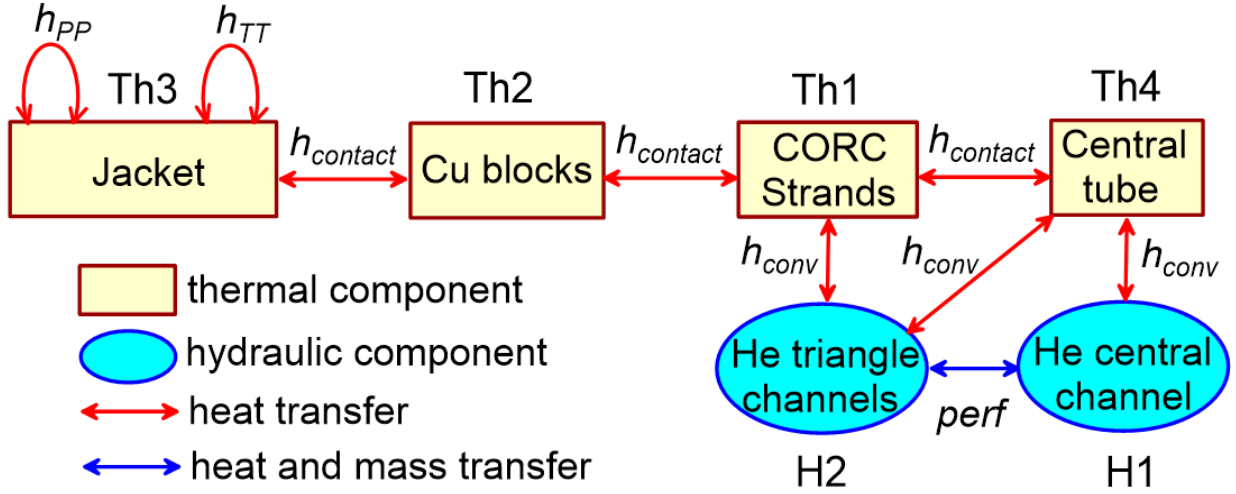
# MF profiles along the selected cable

- Based on the results of the electromagnetic analysis, the magnetic field profiles along several selected HTS cables at the 10 selected time points of the current scenario were determined. For times between these points, the MF was obtained by linear interpolation.
- Simulations of the selected HTS cables under normal operating conditions during the entire current scenario was performed [1], aimed at estimating the minimum temperature margin.
- We identified **cable 16**, located on the top of the HTS1L module, as the one operating under the most demading conditions and featuring the lowest minimum $\Delta T_{marg}$. We selected this cable for the subsequent quench analysis.



# THEA model – 1D conductor components






*Conductor components in the THEA model and thermal links between them*

- Assumed cooling conditions: $T_{in}$ = 4.2 K, $p_{in}$ = 5 bar, we selected $p_{out}$ = 4.774 bar to ensure the correct nominal mass flow rate of 14 g/s
- Thermal links between the conductor components were assumed as in TH simulations of the EU-DEMO conductors [2]:
  - Standard friction factor and heat transfer correlations for flow in the central tube and triangle channels,
  - Contact heat transfer coefficient between the solid cable components $h_{contact}$ = 500 W/(m$^2$K),
  - Perforation of the central tube $\sim 1.5\%$.
- Inter turn (TT) and inter pancake (PP) coductive heat transfer through the GE insulation layer were taken into account: $h_{TT} = h_{PP} = \lambda(T_{ref})/d$.

[2] L. Savoldi and R. Zanino, Common approach for thermal-hydraulic calculations, Memo for WPMAG-2.1-D01 (2016) EFDA_2LMECE

# THEA model – $I_c$ (B,t) scaling law for SST tapes

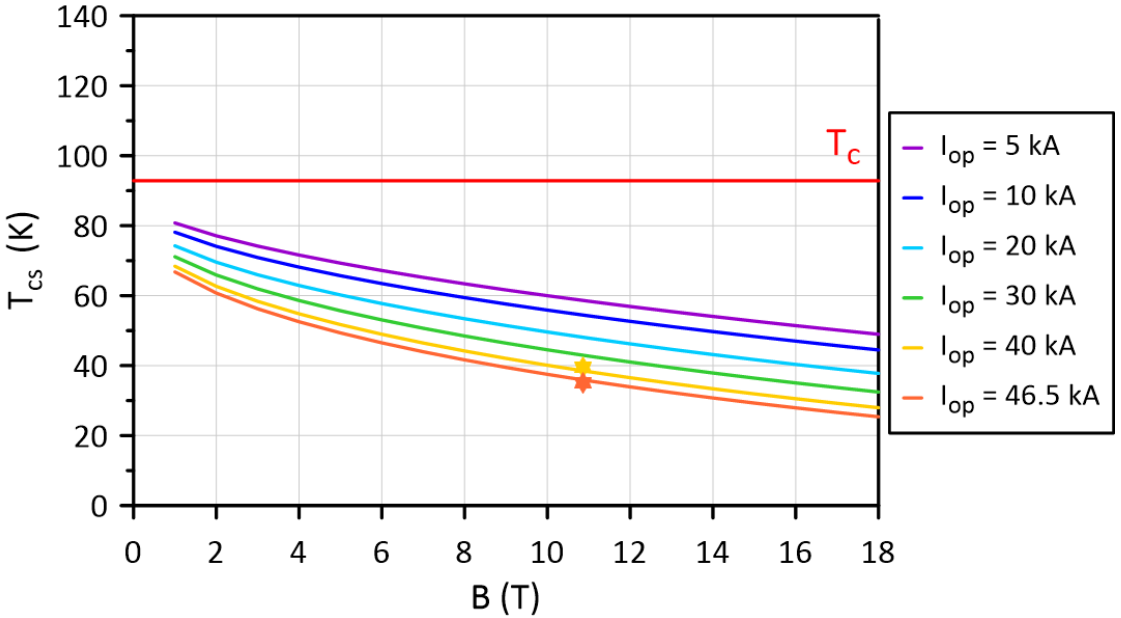
We use the scaling law for SST tapes in the form proposed in [3] (2017):

$$I_c(B,T) = \frac{n_t F_{p0}}{B}\left[\frac{B}{B^*_{sc}(T)}\right]^p \left[1-\frac{B}{B^*_{sc}(T)}\right]^q$$

$$F_{p0}(T) = A_0\left[1-\left(\frac{T}{T_c}\right)^\beta\right] B^*_{sc}(T)^\nu$$

$$B^*_{sc}(T) = B_{sc0}\left[1-\left(\frac{T}{T_c}\right)^\alpha\right]^\mu$$

where: $B_{sc0}$ = 187.7 T, $T_c$=92 K, $\beta$ =6.87, $\alpha$ = 0.514, $\mu$ = 1.496, $\nu$ = 1.514, p = 0.521, q = 1.9.




*$T_{cs}$ as a function of MF obtained with the scaling law. The experimental values measured in SULTAN at 10.85 T for the conductor prototype [4] are indicated by the star symbol.*

The original value $A_0$ = 21.24 $AT^{1-\nu}$/cm [3] was replaced with **$A_0$=49.33 $AT^{1-\nu}$/cm** to get the best agreement with the experimental $T_{cs}$ values [4].

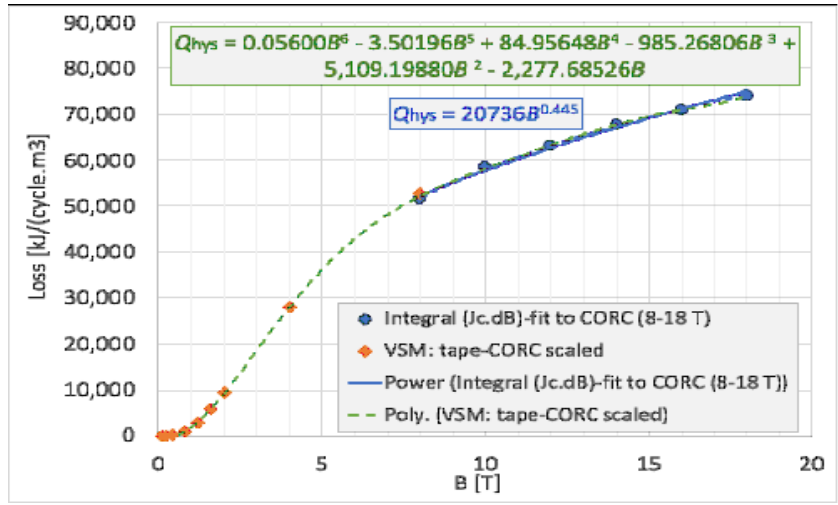

[3] R. Wesche: Ic(B,T) Scaling of Coated Conductors, EPFL-SCP internal report, May 2017

[4] X. Guanyu, *Progress on HTS magnet technology development*, presented at the Seminar on High-Temperature Superconducting Magnets within EU-CN Cooperation, Shanghai, 07.11.2025

# THEA model - heat loads: hysteresis losses

The magnetization loss (in kJ/m$^3$/cycle), normalized to the HTS tapes volume) was calculated based on the experimental fit obtained for the CORC conductor designed by ASIPP [5]:

$$Q_{hys}(B) = \begin{cases} c_1 B^3 & \text{for } 0 < B < 0.903 \text{ T} \\ aB^6 + bB^5 + cB^4 + dB^3 + eB^2 + fB & \text{for } 0.903 \text{ T} < B < 13.369 \text{ T} \\ a_1 B^{b_1} & \text{for } 13.369 \text{ T} < B < 18 \text{ T} \end{cases}$$




where: a = 0.05600, b = -3.50196, c = 84.95648, d = -985.26806, e = 5 109.19880, f = - 2 277.68526, $a_1$ = 20736, $b_1$ = 0.445, $c_1$ = 1953.4.

The respective expression for the thermal power of hysteresis losses (in kW/m) is:

$$P_{hys}(B) = C_{phase} A_{tapes} \frac{dQ_{hys}}{dt} \qquad C_{phase} = 0.25$$

$$P_{hys}(B) = C_{phase} A_{tapes} \left|\frac{dB}{dt}\right| \begin{cases} 3c_1 B^2 & \text{for } 0 < B < 0.903 \text{ T} \\ 6aB^5 + 5bB^4 + 4cB^3 + 3dB^2 + 2eB + f & \text{for } 0.903 < B < 13.369 \text{ T} \\ a_1 b_1 B^{(b_1 - 1)} & \text{for } 13.369 \text{ T} < B < 18 \text{ T} \end{cases}$$

[5] A. Nijhuis, EU-CN CORC-CICC coupling loss in transverse and parallel AC field, Task MAG-T.01.01-T026-D001 (2023), EFDA_D_2RD8QR

# THEA model - Heat loads: coupling and eddy current losses

The coupling loss per unit length of conductor in a field ramped at a uniform rate was calculated as [6]:

$$P_{coupling}(x) = \frac{n\tau S}{\mu_0}\left(\frac{dB(x)}{dt}\right)^2 = \frac{n\tau S}{\mu_0}\left[\left(\frac{dB_r(x)}{dt}\right)^2 + \left(\frac{dB_z(x)}{dt}\right)^2\right]$$

where $n$ - demagnetization factor,

$\tau$ - time constant

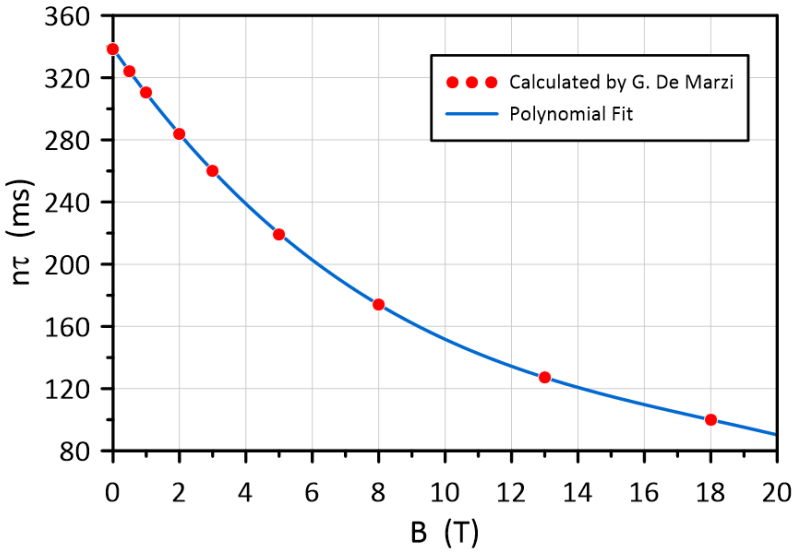
$S$ – copper cross section in a given thermal component.

The values of $\dot{B}_r(x)$ and $\dot{B}_z(x)$ during the subsequent phases of the current scenario were estimated using the respective $B_r\ (x)$ and $B_z(x)$ values at the beginning and end of the given phase.

The $n\tau$ values for the considered conductor geometry, taking into account both the coupling and eddy current losses in the copper components, were obtained by Gianluca De Marzi with a dedicated electrostatic FEM model (assuming copper RRR = 50 and the electrical contact resistance between different cable components equal to: $R_c = 3 \cdot 10^{-7}\ \Omega \cdot m$)

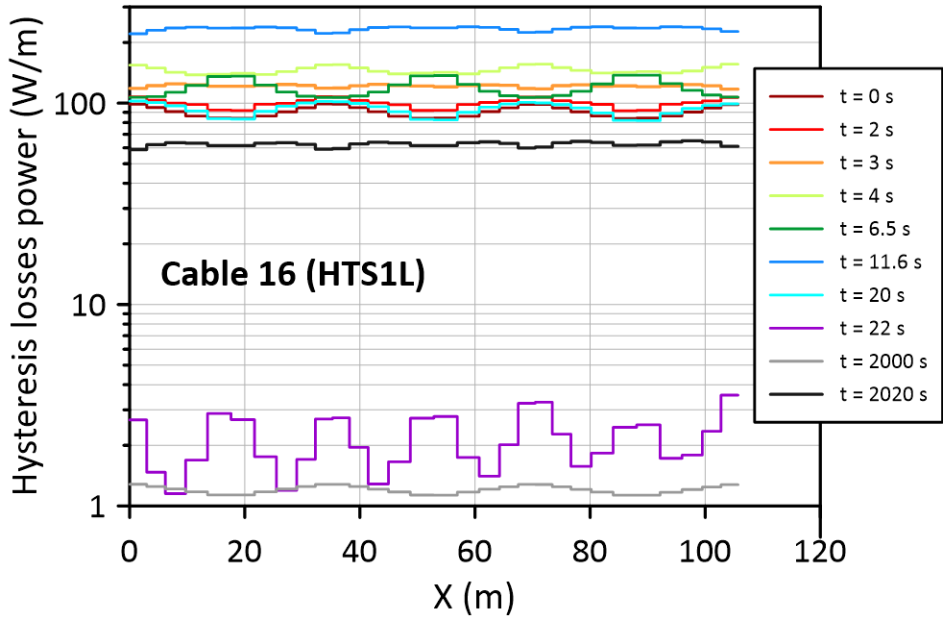
$$\boldsymbol{n\tau\ (B) = -0.0259247 \cdot B^3 + 1.40531 \cdot B^2 - 30.1608 \cdot B + 338.722}$$

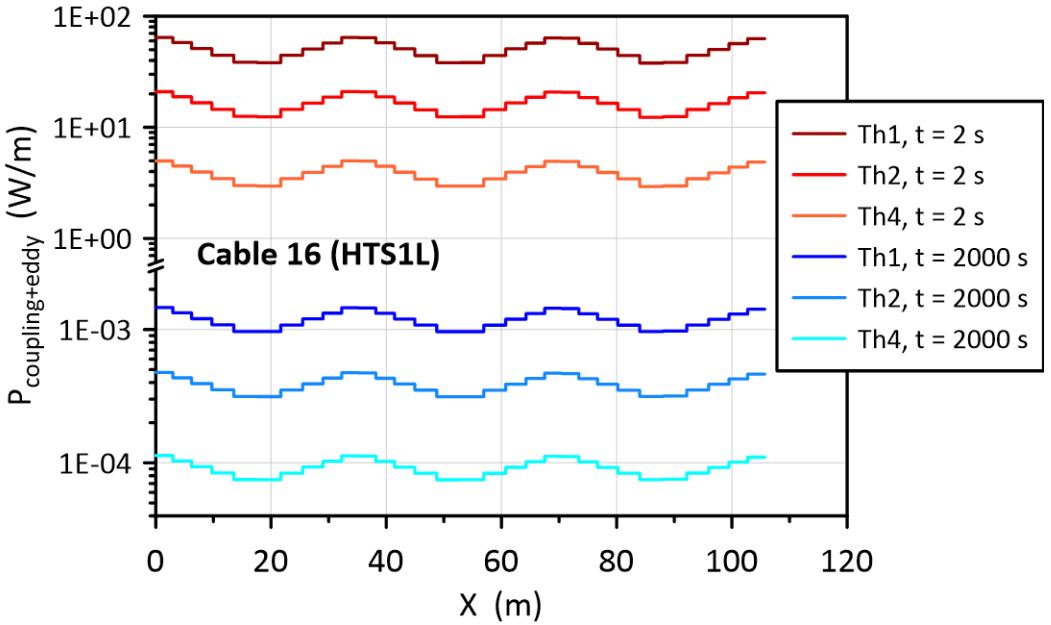
($B$ in T, $n\tau$ in ms)




[6] M. N. Wilson, Superconducting Magnets, Clarendon Press 1983.

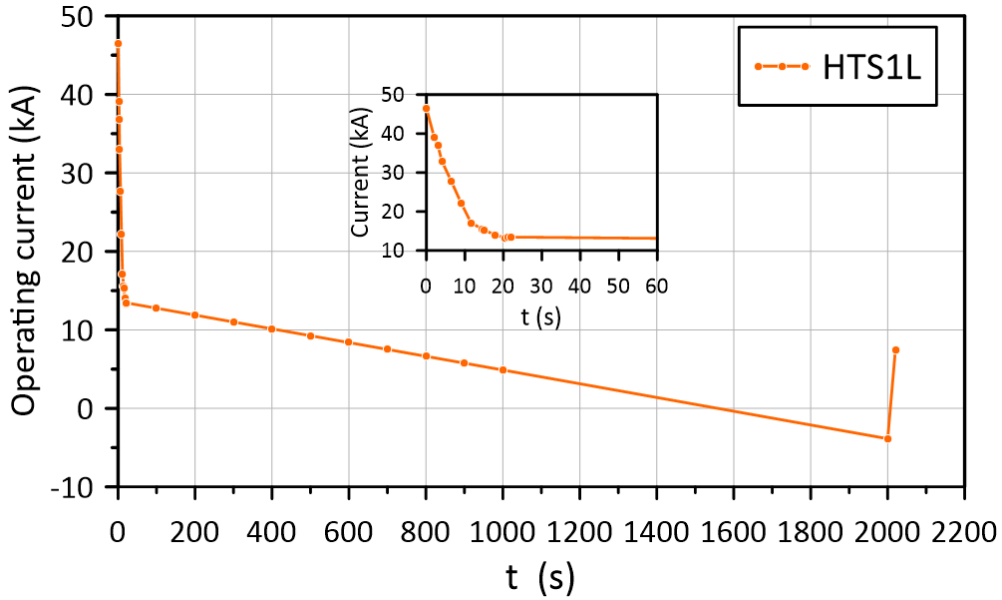
# THEA model - Heat loads at normal operation - examples

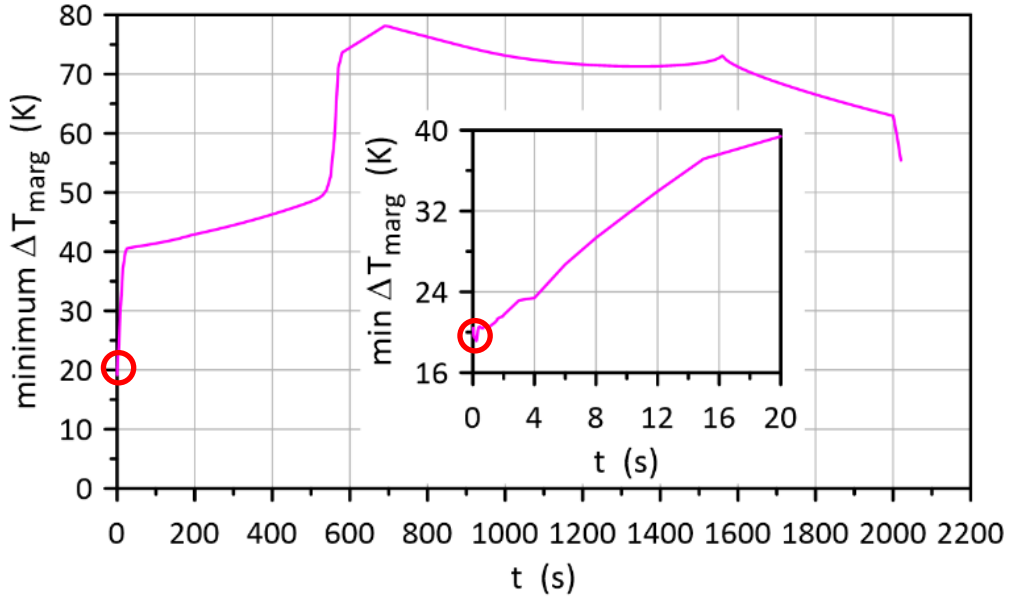



Hysteresis losses in the considered conductors are large, particularly in the first and last few seconds of the current scenario. The coupling and eddy current losses are smaller, but at the beginning of the current scenario they are also quite significant.

# min $\Delta T_{marg}$ evolution in cable 16 during the entire current scenario



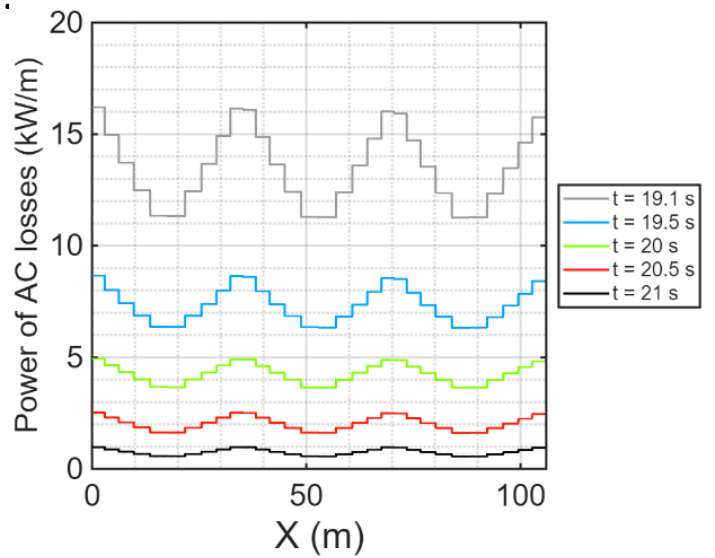

*Time evolution of the min $\Delta T_{marg}$ in cable 16 during the whole current scenario and its exargerated initial part.*

The global minimum (in time and space) of $\Delta T_{marg}$ was observed at the very beginning of the current scenario, where the current and MF are the highest, thus $T_{cs}$ is the lowest.

**Initial state was identified as the moment when quench is most likely to occur.**

# Quench simulations – assumptions (I)

- Quench was initiated by a heat disturbance of energy $E_{pulse}$, length 10, 20, or 30 cm and duration 100 ms.
- Heat pulse triggering quench was imposed at a distance x = 29.6 m, 33.6 m (minimum $\Delta T_{marg}$), or 54.6 m (maximum $\Delta T_{marg}$) from the helium inlet.
- Refined initial mesh with automatic adaptivity with the refined region around the disturbance location was used (Initial mesh: dx = 2.5 cm, in the refined region of 4 m: dx = 0.25 cm).
- The quench detection threshold was set at **0.1 V**, with an additional delay of **1.5 s** (corresponding to typical time necessary for reaction of the quench protection system) before the start of exponential current dump at $t = t_{dump}$ with the characteristic time $\tau_{dump}$ **= 0.814 s** [7].
- During the fast discharge the magnetic field was dumped proportionally to the operating current.
- Heat generation during the fast discharge due AC losses was taken into account.
- Inter-turn and inter-pancake heat transfer was taken into account.




[7] Y. Chen, et al., *Simulation of Quench Behavior in CS LTS Magnets for Next-Generation Fusion Devices With Time-Varying Operation*. IEEE Trans. Appl. Supercond. 35 (2025) Art. No. 4203209.

# Quench simulations – assumptions (II)

**Two quench initiation scenarios were considered:**

| | I phase | II phase |
|---|---|---|
| **Case A** | Constant current ($I_{op}$ = 46.5 kA) and magnetic field profile corresponding to the initial state (t = 0 s) | Exponential current dump if the voltage threshold was reached (after additional delay $t_{delay}$ = 1.5 s) |
| **Case B** | Current and MF following their normal operating scenario | |

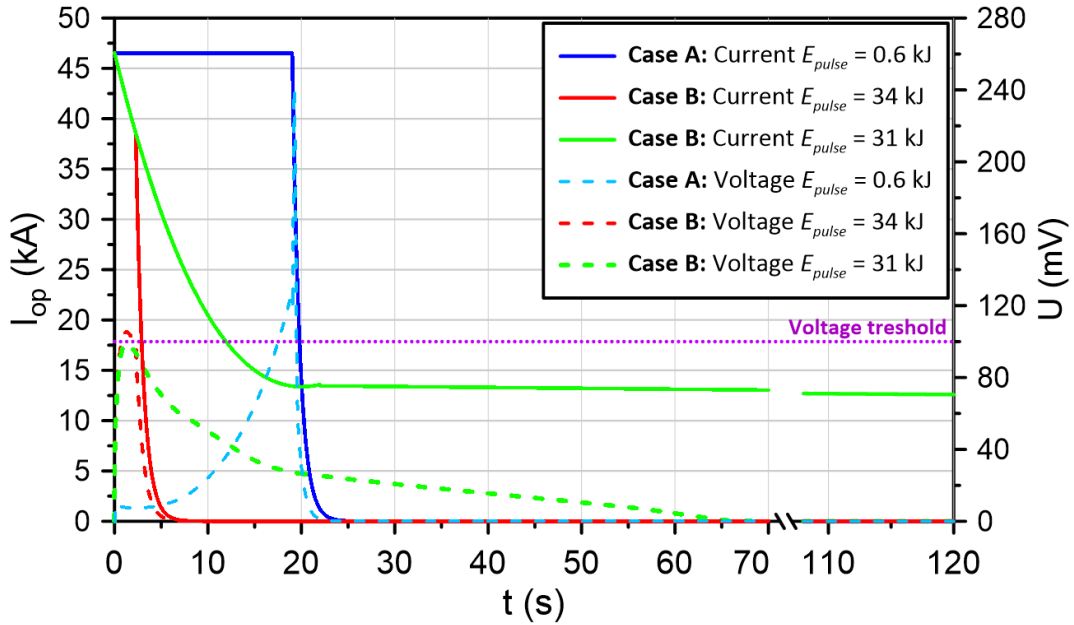
$$I(t) = I_{dump}\, exp\left(-\frac{t-t_{dump}}{\tau_{dump}}\right)$$

$$B_i(x,t) = B_{dump}(x)\, exp\left(-\frac{t-t_{std}}{\tau_{dump}}\right),\ i = r,z,$$

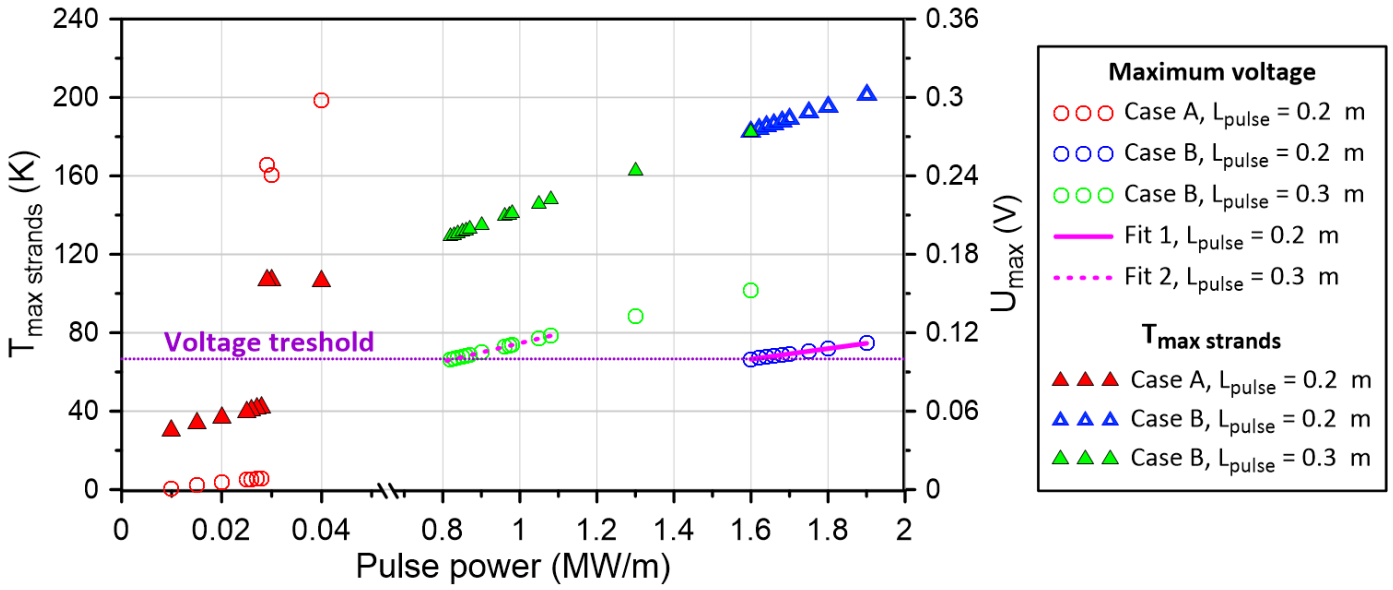
$t_{dump}$ - the time at which the current dump starts

$t_{dump} = t_{detection} + t_{delay}$

$I_{dump}$ and $B_{dump}(x)$ are the current and MF profile at the start of the current dump (i.e. at $t = t_{dump}$)



# Quench simulations – estimation of MQE (cases A&B)

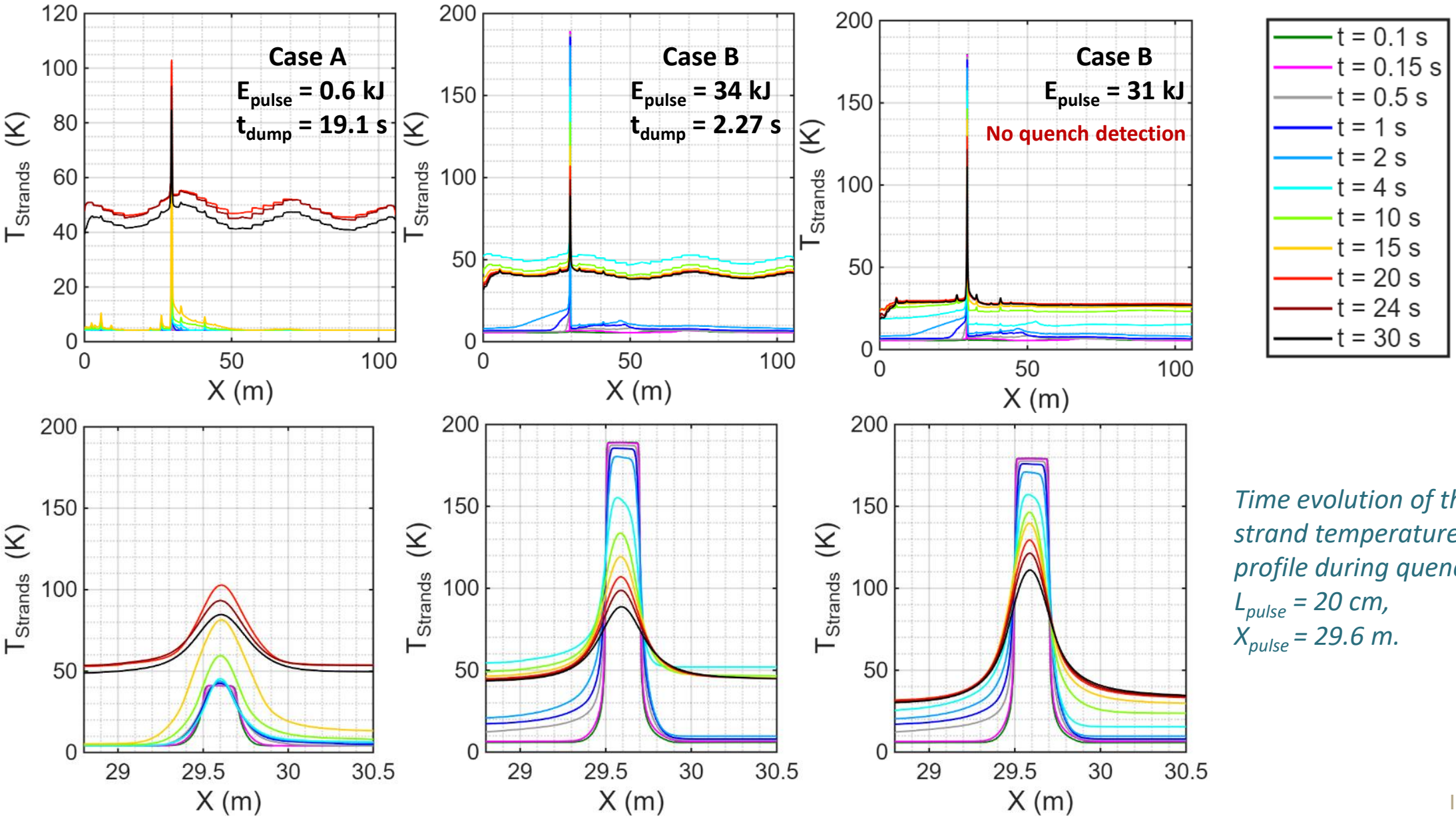



*Maximum strand temperature and maximum voltage as functions of pulse power for two quench scenarios: Case A (constant current prior to current discharge) and Case B (nominal current evolution prior to discharge); $L_{pulse}$ = 20 cm, $X_{pulse}$ = 29.6 m.*

| Case | Pulse length (m) | Min. quench pulse power $P_{pulse}$ (MW/m) | uncertainty $u(P_{pulse})$ | MQE (kJ) | uncertainty u(MQE) (kJ) |
|---|---|---|---|---|---|
| A | 0.2 | 0.0290 | 0.0010 | 0.580 | 0.021 |
| B | 0.2 | 1.605 | 0.011 | 32.09 | 0.45 |
| B | 0.3 | 0.8303 | 0.0037 | 24.91 | 0.34 |

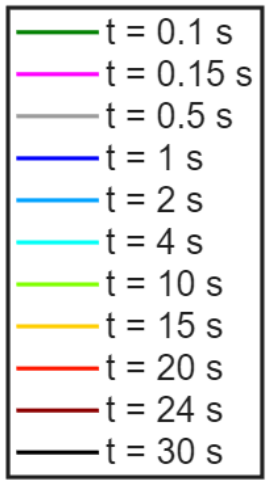
- Very large MQE in case B results from the fast increase in $T_{cs}$ at the beginning of the nominal scenario, where both MF and current decrease rapidly.
- MQE decreases when the pulse length increases, particularly in Case B.

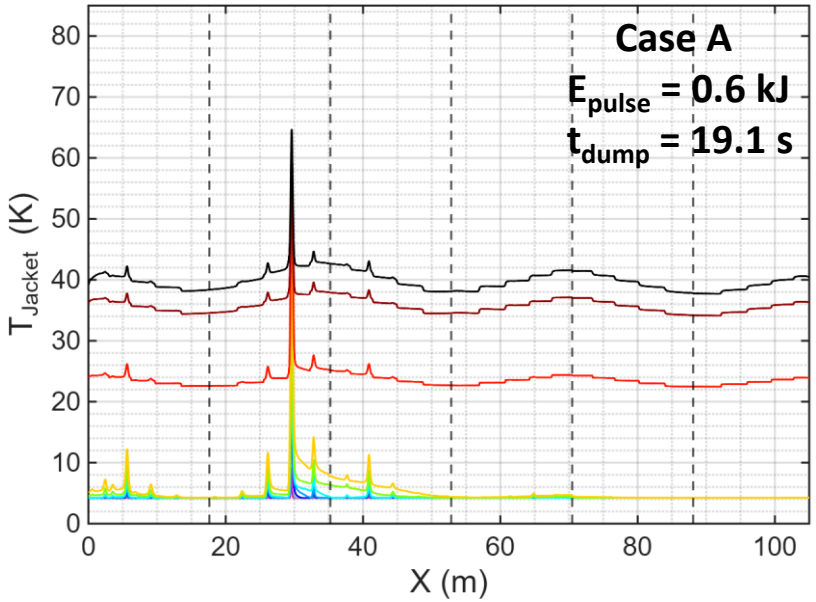
# Results: typical strand temperature evolution



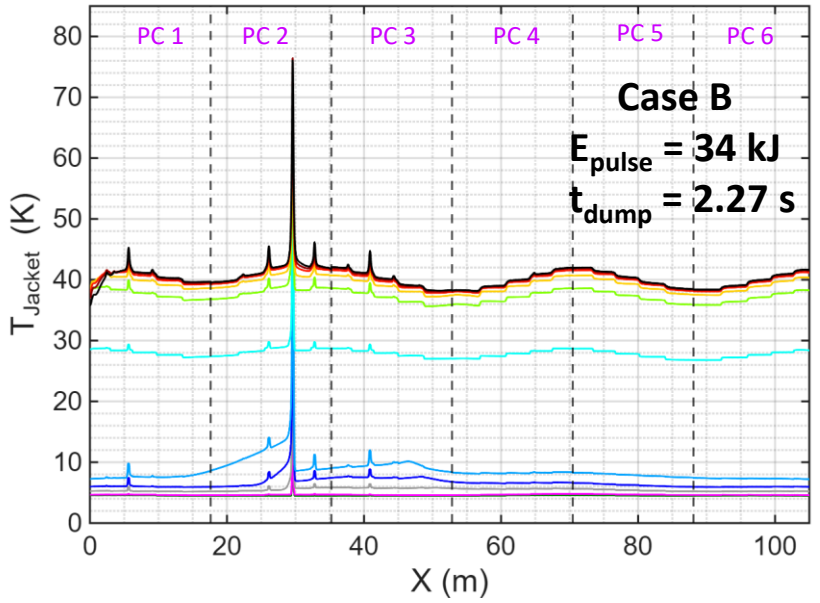

*Time evolution of the strand temperature profile during quench;*
*$L_{pulse}$ = 20 cm,*
*$X_{pulse}$ = 29.6 m.*

# Results – Evolution of the jacket temperature



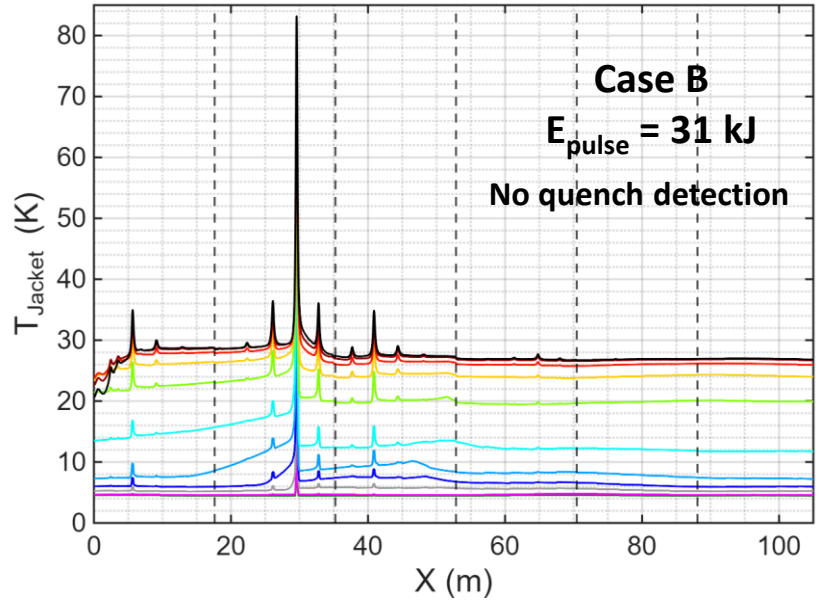

PC - pancake




Local temperature peaks occur due to the transverse heat transfer.

The hot-spot temperature of the jacket were well below the acceptable limit of 150 K, However, in case B the strand temperature was relatively high, **even when quench was not detected**, which calls for attention of the conductor designers.

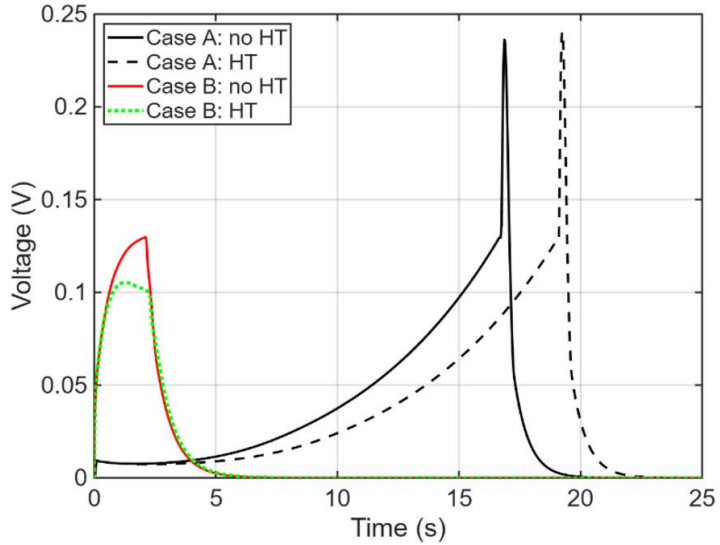
| | $E_{pulse}$ (kJ) | $T_{strand\ max}$ (K) | $T_{jacket\ max}$ (K) |
|---|---|---|---|
| Case A | 0.6 | 106.9 | 64.7 |
| Case B | 34 | 189.5 | 76.4 |
| Case B | 31 | 179.5 | **83.2** |




*Time evolution of the jacket temperature profile during quench; $L_{pulse}$ = 20 cm, $X_{pulse}$ = 29.6 m.*

# Results – effect of the transverse (T-T and P-P) heat transfer on the hot spot temperature

| Case | TT&PP heat transfer | $E_{pulse}$ (kJ) | $T_{max\ jac}$ (K) | $T_{max\ strand}$ (K) | $t(T_{max\ strand})$ (s) | $t_{dump}$ (s) |
|---|---|---|---|---|---|---|
| Case A | No HT | 0.6 | 70.38 | 104.74 | 16.70 | 16.66 |
| Case A | HT | 0.6 | 64.67 | 106.91 | 19.07 | 19.03 |
| Case B | No HT | 34 | 86.22 | 192.71 | 2.16 | 2.12 |
| Case B | HT | 34 | 76.41 | 189.08 | 0.10 | 2.28 |




*Time evolution of the voltage during quench; $L_{pulse}$ = 20 cm, $X_{pulse}$ = 29.6 m.*

- Transverse heat transfer redistributes a considerable fraction of the deposited energy to neighboring turns and pancakes, leading to several effects:
  - Reduction of the local temperature at the quench initiation point,
  - Slower propagation of the primary normal zone,
  - Local temperature peaks in adjacent turns and pancakes, though the large $\Delta T_{marg}$ prevents the formation of additional normal zones,
  - Dealayed voltage build-up resulting in later quench detection.
- Accounting for transverse heat transfer has a moderate effect on the hot spot temperature (by a few K), but this effect acts in opposite directions in Case A and Case B.

# Results – effect of the disturbance location and $\Delta T_{marg}$ on the hot spot temperature ($E_{pulse} \approx 2$ x MQE, $L_{pulse}$ = 20 cm)

| Case | Description | $\Delta T_{marg}$ (K) | $E_{pulse}$ (kJ) | $T_{max\ str}$ (K) | t ($T_{max\ str}$) (s) | X ($T_{max\ str}$) (m) |
|---|---|---|---|---|---|---|
| Case A | Reference | 22.10 | 1.2 | 105.83 | 11.33 | 29.6 |
| Case A | min $\Delta T_{marg}$ | 20.55 | 1.2 | 101.57 | 10.28 | 33.6 |
| Case A | max $\Delta T_{marg}$ | 27.34 | 1.2 | 121.45 | 29.07 | 54.6 |
| Case B | Reference | 22.1 | 68 | 290.38 | 1.81 | 29.6 |
| Case B | min $\Delta T_{marg}$ | 20.55 | 68 | 290.22 | 1.80 | 33.6 |
| Case B | max $\Delta T_{marg}$ | 27.34 | 68 | 290.26 | 0.10 | 54.6 |

**Case A:**

- Hot-spot temperature scales with the local temperature margin (larger margin => higher peak temperature).
- Mechanism: Larger temperature margin => slower normal zone propagation => later quench detection => extended Joule heating,
- The hot spot temperature for $E_{pulse} \approx 2$ x MQE almost the same as for $E_{pulse} \approx$ MQE.

**Case B:**

- Maximum strand temperature remains constant (~290 K) across all pulse locations,
- Mechanism: Response driven by the huge deposited energy,
- The hot-spot temperature significantly higher for $E_{pulse} \approx 2$ x MQE than for $E_{pulse} \approx$ MQE.

# Results – effect of the disturbance length on the hot spot temperature ($E_{pulse} \approx 2$ x MQE, $X_{pulse} = 29.6$ m)

| | $P_{pulse}$ (kW/m) | $L_{pulse}$ (m) | $E_{pulse}$ (kJ) | $T_{max\ str}$ (K) | t ($T_{max\ str}$) (s) |
|---|---|---|---|---|---|
| Case A | 60 | 0.2 | 1.2 | 105.83 | 11.33 |
| Case A | 120 | 0.1 | 1.2 | 109.79 | 12.27 |
| Case B | 3400 | 0.2 | 68 | 290.38 | 1.81 |
| Case B | 6800 | 0.1 | 68 | 480.05 | 0.10 |

**Case A:**

- Low Sensitivity: Only moderate differences in peak temperature (of a few K) and discharge time between 10 cm and 20 cm disturbances.
- Mechanism: Driven by slow voltage build-up, peak temperature is dominated by pre-discharge Joule heating.

**Case B:**

- High Sensitivity: Strong dependence on localization – reducing length from 20 cm to 10 cm (at constant $E_{pulse}$) increases peak temperature from 290 K to 480 K.
- Mechanism: Higher energy density in localized zones causes severe local overheating.:

**Conclusion:** **Very localized disturbances yield substantially higher hot-spot temperatures**.

**Proposed future approach:** modeling of realistic local degradation, e.g. by implementing spatially dependent scaling law $J_c(B,T,x)$ to account for local damage, manufacturing defects, or cross-section degradation. Create a framework for evaluating highly localized quench scenarios in HTS fusion magnets.

# Summary, conclusion and perspectives

- THEA model of the BEST CS HTS conductor, and the dedicated UserMagneticField, UserCurrent and UserSHeating procedures for simulations of conductors' quench operation have been prepared. The model accounts for heat loads due to AC losses during the current dump, as well as inter-turn and inter-pancake heat transfer.
- Quench simulations were performed for Cable 16 (located on the top of the HTS1L module) - the cable operating under the most demanding conditions, with the lowest minimum temperature margin.
- In quench simulations two scenarios prior to current dump were considered: Case A with constant current ($I_{op}$ = 46.5 kA) and a constant MF profile corresponding to the initial state, and Case B with current and MF following their nominal scenarios.
- Effects of location, energy, and spatial length of the heat disturbance on the hot spot temperature were studied
- In Case B, it was very difficult to reach the threshold voltage, even if the normal zone with a relatively high hot-spot temperature was formed. This is due to the large temperature margin and the fast increase of $T_{cs}$ at the beginning of the nominal scenario, when both the magnetic field and the current decrease rapidly. As a result, the estimated MQE was very high and the normal zone propagation velocity was very low.
- Despite the high MQE value, in most of considered cases the hot-spot temperatures of the jacket were well below the acceptable limit of 150 K.
- Because of the very large temperature margin, the formation of a normal zone by heat disturbances is unlikely. However, if it does occur, the observed problems with detecting highly localized normal zones may pose a risk of strand damage. **Alternative quench detection methods that provide more reliable early indication of quench initiation,** or perhaps reduction in the voltage threshold could be considered by the coil designers.
- The analysis of heat transfer between the HTS and LTS parts during normal coil operation to evaluate the impact of the HTS section on the LTS conductors is ongoing.

# Thank you very much for your attention

*This work has been carried out within the framework of the EUROfusion Consortium, funded by the European Union via the Euratom Research and Training Programme (Grant Agreement No 101052200 — EUROfusion). Views and opinions expressed are however those of the author(s) only and do not necessarily reflect those of the European Union or the European Commission. Neither the European Union nor the European Commission can be held responsible for them.*
*This work has been co-financed by the Polish Ministry of Science and Higher Education in the framework of the International Co-financed Projects (PMW) programme in the years 2025 (contract number 6265/HE - EURATOM/2025/2) and 2026.*